Effects of niobium content on electrical and mechanical properties of $(Na_{0.85}K_{0.15})_{0.5}Bi_{0.5}Ti_{(1-x)}Nb_xO_3$ thin films

**Li Xujun · Pan Yong · Gong Yueqiu ·
Huang Renjie · Liao Jiajia · Xie Shuhong ·
Zhou Yichun · Gao Xingsen**

Abstract $(Na_{0.85}K_{0.15})_{0.5}Bi_{0.5}Ti_{(1-x)}Nb_xO_3$ (NKBT-N100x) thin films were deposited on Pt/Ti/SiO$_2$/Si(100) substrates by metal–organic decomposition method and annealed in oxygen atmosphere at 750 °C. The effects of niobium concentration on the microstructures, ferroelectric, piezoelectric, leakage current and mechanical properties of the NKBT-N100x ($x = 0$, 0.01, 0.03, 0.05) thin films have been investigated in detail. The NKBT-3N thin film has the largest remnant polarization (7 μC/cm^2) and statistically averaged d_{33eff} (140 pm/V), the smallest leakage current, elasticity modulus (102.0 Gpa), hardness (5.1 Gpa) and residual stress (297.0 Mpa). The evaluation of residual stresses of these thin films will offer useful guidelines of safe working condition for their potential application in microelectromechanical system.

1 Introduction

Lead-free piezoelectrics are desired inevitably as alternatives for lead-based materials for the sake of environmental

L. Xujun · P. Yong · G. Yueqiu (✉) · H. Renjie · L. Jiajia ·
X. Shuhong · Z. Yichun
Faculty of Materials, Optoelectronics and Physics, Xiangtan
University, Xiangtan 411105, China
e-mail: yqgong@xtu.edu.cn

L. Xujun · P. Yong · G. Yueqiu · X. Shuhong · Z. Yichun
Key Laboratory of Low Dimensional Materials and Application
Technology, Ministry of Education, Xiangtan University,
Xiangtan 411105, China

G. Xingsen
Institute for Advanced Materials, School of Physics and
Telecommunications Engineering, South China Normal
University, Guangzhou 510631, China

protection and biocompatibility since lead toxicities during producing, using and recycling are problematic for devices associated with PbZrO$_3$–PbTiO$_3$ and other lead-based piezoelectrics [1]. Thus, there is an increasing interest in developing lead-free piezoelectrics.

Na$_{0.5}$Bi$_{0.5}$TiO$_3$ (NBT) is a kind of perovskite-type piezoelectrics. For its strong ferroelectricity at room temperature [2, 3], NBT has been considered to be a good candidate for lead-free ferroelectrics. However, its piezoelectric property is too low to be practically used because of its high electrical conductivity. To improve its piezoelectric property, a variety of modifications with other perovskite compounds have been carried out [4–14]. The $(1-x)$NBT-x(K$_{0.5}$Bi$_{0.5}$)TiO$_3$ (NKBT100x) thin films have received considerable attention due to their excellent ferroelectric and piezoelectric properties near the rhombohedral-tetragonal morphotropic phase boundary (MPB) at $0.13 \leq x \leq 0.17$ [11]. As the NKBT15 thin film shows the best properties [11], we selected NKBT15 as the doped object.

Sodium–potassium niobate has been expected as another promising candidate for high performance lead-free piezoelectric material because of its high planar coupling coefficient, high Curie temperature, moderate dielectric permittivity and high piezoelectric constant [15]. Recently, the Nb-doped NKBT100x ceramics have reported with improved dielectric and ferroelectric properties [16]. However, there are few reports about the effects of niobium content on the properties of NKBT100x thin films. Therefore, the purpose of the present study is to investigate the effect of various niobium contents on the electrical and mechanical properties of NKBT15 thin film.

In this paper, $(Na_{0.85}K_{0.15})_{0.5}Bi_{0.5}Ti_{(1-x)}Nb_xO_3$ (NKBT-N100x) thin films were deposited on Pt/Ti/SiO$_2$/Si(100) by metal–organic decomposition (MOD) method, and the

effects of niobium content on their microstructures, electrical and mechanical properties were investigated by X-ray diffractometer (XRD), atomic force microscopy (AFM), piezoelectric force microscope (PFM), ferroelectric tester, semiconductor analyzer and nanoindentater. The evaluation of residual stress for NKBT-N100x thin films and its effects on their electrical properties are expected to offer useful guidelines to the design and application of other lead-free ferroelectric thin films.

2 Experimental

2.1 Sample preparation

NKBT-N100x thin films were prepared by MOD process with rapid thermal annealing. Stoichiometric amounts of sodium acetate (≥99.0 %, AR), potassium acetate (≥92.0 %, AR), bismuth acetate (≥99.99 %, AR), ethanol niobium (≥99.99 %, AR) and tetrabutyl titanium (≥99.5 %, AR) were selected as staring materials. Acetic acid (≥99.9 %, AR) and 2-methoxyethanol (≥99.5 %, AR) with volume ratio of 1:1 were chosen as co-solvent. During the preparation, the ethanol niobium was dissolved firstly in the above co-solvent with protective gas in order to prevent the hydrolysis of ethanol niobium caused by the moisture in the environment, and it is named as precursor solution A. Stoichiometric amounts of sodium acetate, potassium acetate and bismuth acetate were also dissolved in the above mentioned co-solvent to form precursor solution B. To compensate for the volatility of Bi, Na, and K in the annealing process, all these three starting materials were taken in a 10 % excess amount (mol %). The precursor solution B was constantly stirred until a transparent and stable clarified precursor solution was obtained. Precursor solution A and tetrabutyl titanium were added to the precursor solution B with continuous stirring until the final mixture became a stable yellow precursor with a molar concentration of 0.25 mol dm^{-3}. The mixed precursor solution was deposited on Pt/Ti/SiO$_2$/Si(100) substrates by spin coating at 300 rpm for 8 s and 3,000 rpm for 40 s. After each spin-on deposition, the wet thin films were dried at 150 °C for 120 s, pyrolysed at 400 °C for 300 s and annealed at 750 °C for 600 s in oxygen atmosphere by a rapid thermal annealing furnace (RTP-500, Beijing Institute of Applied Physics, China). The spin coating and heat-treatment were repeated for 10 times to obtain the desired thickness. In order to measure the electrical properties, circular Pt top electrodes of diameter 0.2 mm were sputtered on the surface of these thin films using a shadow mask by dc magnetron sputtering, thus Pt/NKBT-N100x thin films/Pt capacitors were obtained.

2.2 Structural characterization and performance analysis

The NKBT-N100x ($x = 0, 0.01, 0.03, 0.05$) thin films were measured by grazing incidence XRD (D/Max 2550 VB, Rigaku, Japan). X-ray radiation source was Cu K_α with the wavelength of 0.15406 nm, and the scanning angle was in the region of 20–65° and the fixed angle of grazing incidence X-ray is 3°. The thin films were scanned at 4°/min with an increment degree of 0.02°.

The surface morphology of NKBT-N100x ($x = 0, 0.01, 0.03, 0.05$) thin films were characterized by AFM (SPM-9500, Shimazu, Japan).

The ferroelectric properties of NKBT-N100x ($x = 0, 0.01, 0.03, 0.05$) thin films were analyzed by RT66A analyzer, and the piezoelectric properties were examined by PFM (Asylum Research MFD-3D AFM, Oxford Instruments plc, USA). The current–voltage (I–V) measurements were performed by using Agilent B1500 semiconductor analyzer (Agilent Technologies, Inc, USA) under both negative and positive voltage sweeps.

The nanoindentater (TriboIndenter, Hysitron, USA) was used to investigate the mechanical properties of NKBT-N100x thin films. The linear loading and unloading were fixed at the same rate of 0.5 μN/s. All nano-indents were performed at the thermal drift less than 0.01 nm/s. The elastic modulus could be obtained from the unloading part of load–displacement curve using Oliver and Pharr method [17].

Using a $\sin^2\psi$ method, in-plane residual stress of thin film was determined by the change of lattice parameter d depending on the tilt angles ψ of the lattice plane [18]. Using ten different X-ray incidence angles, the high degree peaks around 46° in the XRD pattern, the NKBT-N100x thin films were scanned at 0.25°/min with an increment degree of 0.02°. All the tests were carried out at room temperature.

3 Results and discussion

3.1 Microstructures

Figure 1 presents the XRD patterns of the NKBT-N100x ($x = 0, 0.01, 0.03, 0.05$) thin films in the 2θ range of 20°–65°. When $x \leq 0.03$, a single perovskite structure without any second impurity phases could be confirmed, indicating that the Nb^{5+} successfully diffused into the lattice of the NBKT15 thin film to form solid solution. As shown in Fig. 1, the peaks located around 32° and 40° for the NKBT-1N thin film are the sharpest, which indicates that the NKBT-1N thin film has the best crystallinity. For the NKBT-3N thin film, all the peaks are diffused, especially for the peak located at 32°, which means that there is
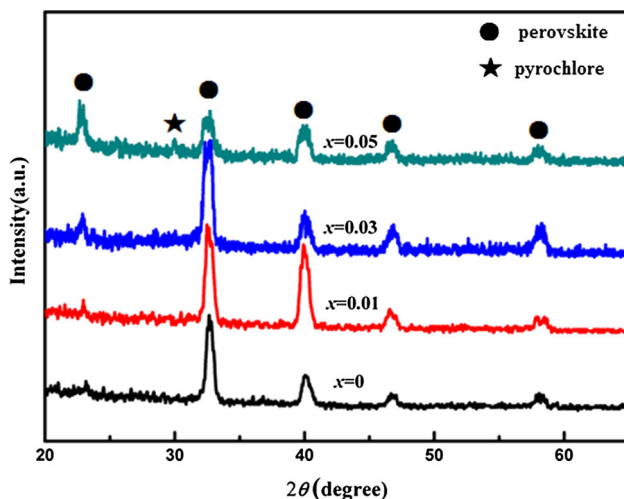
typical phase coexistence. For the NKBT-5N thin film, there is a pyrochlore phase ($Bi_2Ti_2O_7$) (JCPDS, File No.32-0118) [19]. It may be caused by the fact that the substitution of Nb for Ti led to the formation of $Bi_2Ti_2O_7$ according to the following two chemical reactions [20]:

$$Na_2O + K_2O + 2Nb_2O_5 = 4Na_{0.5}K_{0.5}NbO_3 \quad (1)$$

$$Bi_2O_3 + 2TiO_2 = Bi_2Ti_2O_7 \quad (2)$$
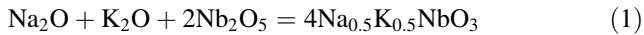
This suggested that the solubility limit of Nb in NKBT100x thin films was between 0.03 and 0.05. This is similar to $Bi_{3.25}La_{0.75}Ti_{3-x}Nb_xO_{12}$ thin film, in which the excess of Nb (beyond 0.04) contributes to the formation of the pyrochlore phase [21]. The average grain size of the thin films was calculated according to the Scherrer formula [22]:

$$L = \frac{0.89\lambda}{B\cos\theta} \quad (3)$$

where L, λ, B and θ are the grain size, the wavelength of the Cu K_α radiation, the full width at half maximum of the diffraction peak located at about 46°, and the corresponding Bragg diffraction angle. The average grain sizes are decreased with the increase of niobium content, with the values being 33.1, 30.3, 29.2 and 28.7 nm for the NKBT-N100x thin films with $x = 0$, $x = 0.01$, $x = 0.03$ and $x = 0.05$, respectively. The grain sizes decrease with the increase of niobium content. It can be explained by the creation of A-site cation vacancies, which were created to maintain charge neutrality in the lattice. These cation vacancies existed along grain boundaries, and they were thermodynamically more stable than those inside the grain. Grain boundaries would be pinned by these defects, inhibiting grain growth and resulting in relatively small grains [23]. Additionally, the formation of $Na_{0.5}K_{0.5}NbO_3$

or the pyrochlore phase may be the other reason for the decrease of the grain sizes, because the remaining second phases segregate at the grain boundaries, leading to the inhibition of grain growth [24].

The AFM images (1 μm × 1 μm) of NKBT-N100x ($x = 0$, 0.01, 0.03, 0.05) thin films are plotted in Fig. 2a–d. The surfaces of all the thin films are dense and uniformly distributed grains without any island. The grain sizes of the NKBT-N100x thin films in the figures are relatively small, which may be caused by the rapid thermal processing and the very short annealing time (600 s) which provided enough energy for crystallization but insufficient time for the complete growth of the grains.

3.2 Mechanical properties

The residual stress of ferroelectric thin film should be determined by material parameters such as elastic, dielectric and piezoelectric constants [25]. If elastic modulus and Poisson's ratio can be estimated, the residual stress in NKBT-N100x thin films can be approximately evaluated by the $\sin^2\psi$ method. Using a nano-indentation tester, 250, 500, 750 and 1,000 μN indentation loads were applied to the surface of NKBT-N100x ($x = 0$, 0.01, 0.03 and 0.05) thin films. The typical load–displacement curves of indentations are shown in Fig. 3a–d. The elastic moduli and the hardness can be determined from the load-indentation depth curve using the method of Oliver [17], and these two values versus Nb-contents are summarized in Fig. 3e. They decreased as the increase of niobium


Fig. 1 XRD patterns of NKBT-N100x ($x = 0$, 0.01, 0.03, 0.05) thin films
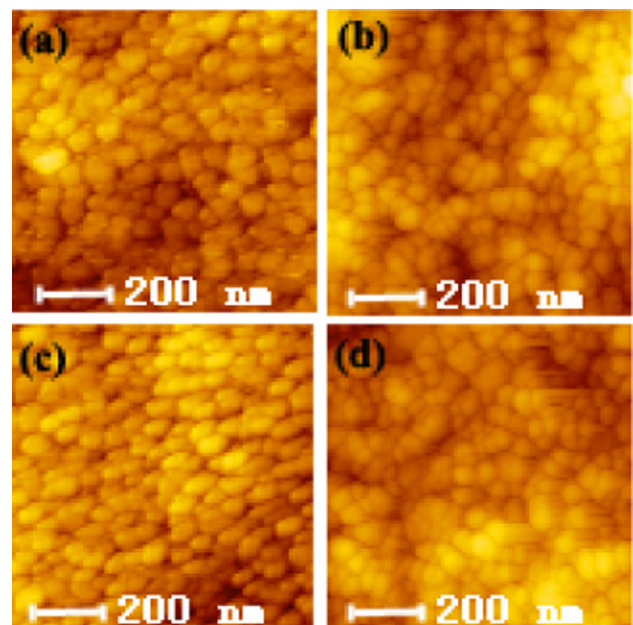
Fig. 2 AFM image of the NKBT-N100x thin film with **a** $x = 0$, **b** $x = 0.01$, **c** $x = 0.03$, **d** $x = 0.05$. The scan size is 1×1 μm^2

contents before 0.03 and increased afterwards because of the phase coexistence. As shown in Fig. 1, there is typical phase coexistence for the NKBT-3N thin film. Owing to the phase coexistence, there is an existence of the different symmetry region (DSR). The movement of DSR boundary increases the elastic compliances [26].

The XRD peaks located at about 46° with different X-ray incident angles ($\psi = 0°, 5°, 10°, 15°, 20°, 25°, 30°, 35°$) for NKBT-N100$x$ thin films ($x = 0, 0.01, 0.03$ and 0.05) are shown in Fig. 4. If we set $2\theta_\psi$ as y-axis, $\sin^2\psi$ as x-axis, and fit the experimental data as a straight line, then the slope can be used to determine the residual stress σ_ϕ. The larger the incident angle is, the more accurate the calculated data are. Therefore, with the above diffraction

spectrum and a Poisson ratio of 0.25 [27], the residual stress of these thin films can be measured by the conventional $\sin^2\psi$ method, and they are 762, 563, 297 and 496 MPa for NKBT-N100x ($x = 0, 0.01, 0.03$ and 0.05) thin films, respectively. It is the residual tensile stress because of the following two possible reasons. Firstly, when the epitaxial strain is neglected in the NKBT-N100x thin films, the in-plane strain in thin film mainly originates from the lattice and thermal expansion mismatches between film/substrate systems [28]. The lattice parameter of Nb-doped NKBT (0.3837 nm) [16] is smaller than that of Pt (0.3924 nm), therefore the lattice mismatch will contribute to the in-plane tensile strain during the crystallization of perovskite phase. Additionally, the

Fig. 3 Typical load–displacement indentation curves of NKBT-N100x thin films with **a** $x = 0$, **b** $x = 0.01$, **c** $x = 0.03$, **d** $x = 0.05$ and **e** the elastic modulus and hardness of NKBT-N100x thin films as a function of niobium content
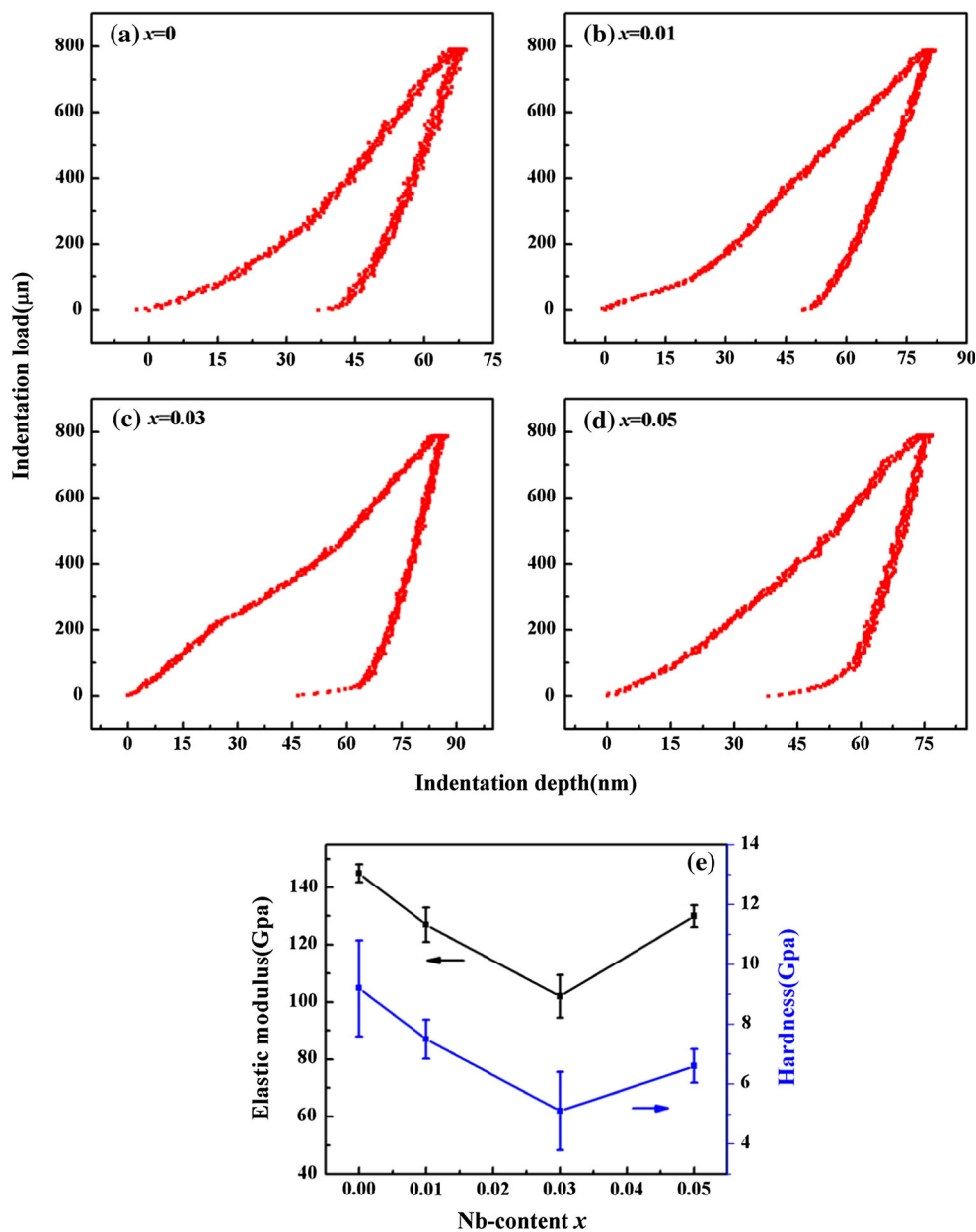
Fig. 4 XRD peaks of high angle plane with different X-ray incident angles for NKBT-N100x thin films with **a** x = 0, **b** x = 0.01, **c** x = 0.03, **d** x = 0.05
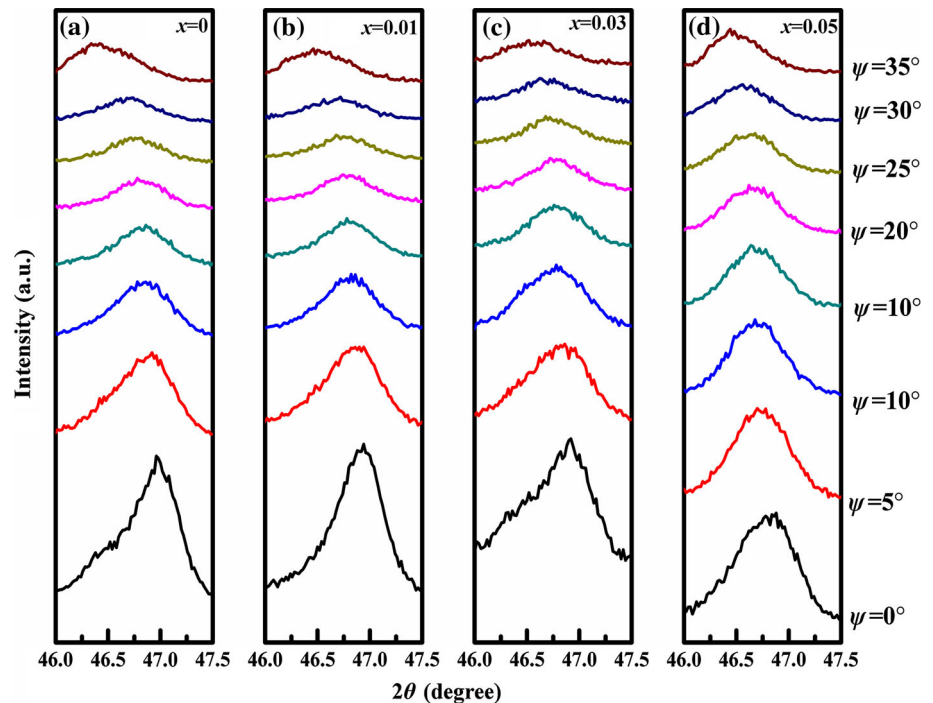
thermal expansion coefficient of NBT-based ceramic (11×10^{-6}/°C) [11] is larger than that of Pt (8.9×10^{-6}/°C) [11], therefore, thermal deformation of NKBT-N100x thin films should be larger than that of Pt substrate, indicating that tensile stress will be induced during the annealing process.

The residual stresses values of the NKBT-N100x thin films are shown in Fig. 5. The residual stresses decrease along with the niobium contents before 0.03 and increase afterwards, and the reasons may be the following two. Firstly, it is the result of the ionic radius difference. As the ionic radius of Nb^{5+} (0.0640 nm) is larger than that of Ti^{4+} (0.0605 nm), the relatively large ionic radius leads to the alleviation of the lattice mismatch between the NKBT-N100x thin films and the Pt substrate. Therefore, the residual tensile stresses decrease along with the niobium contents. Secondly, crystal thermal expansion is due to the expansion of the lattice. Along with the increase of lattice energy, the atom vibration amplitude between the equilibrium positions is increased, and the atomic distance increased accordingly, which led to the emergence of the expansion of the lattice. In ABO_3 structured materials, the perovskite structure deviation factor "t" has the following relation [29]:

$$t = \frac{r_A + r_O}{\sqrt{2}(r_B + r_O)} \qquad (4)$$

where r_A, r_B, and r_O are the ionic radii of the A, B, and oxygen ions, respectively. In the case of the ideal cubic perovskite structure, "t" = 1, and for stable perovskite structure, "t" value is generally $0.8 \sim 1.0$. When lattice
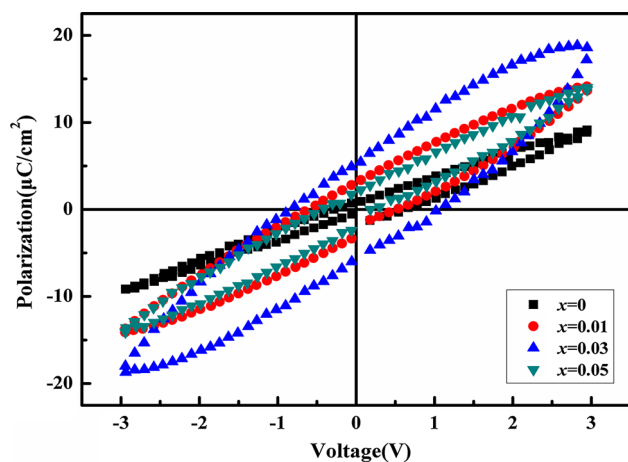
structure is distorted, the "t" value becomes smaller. The distorted perovskite structure leads to the increased lattice energy and enlarged thermal expansion accordingly. The ionic radius of Nb^{5+} is larger than that of Ti^{4+}, which leads to the diminution of the "t" value and the thermal expansion augmented accordingly. This result means that the tensile stress induced by thermal mismatch increases along with the niobium content. However, when the niobium content is more than 0.03, the residual stress value caused by the change of lattice parameter may be smaller than that caused by the change of thermal expansion coefficient, which leads to the increase of the residual stresses for NKBT-5N thin film.

3.3 Electrical properties

Polarization–electric field (P–E) curves of the NKBT-N100x (x = 0, 0.01, 0.03, 0.05) thin films are shown in Fig. 6. The Pt/NKBT-3N/Pt capacitor exhibits a slim type P–E hysteresis loop. The remnant polarization value ($P_r \sim 7$ μC/cm^2) of the NKBT-3N thin film was larger than that of the NBT film ($P_r = 5.4$ μC/cm^2) [30], but it was relatively small compared to that of the NKBT ceramics (~ 34 μC/cm^2) [2] because of the stress between the thin film and Pt/Ti/SiO$_2$/Si substrate. The P_r value of NKBT-N100x (x = 0, 0.01, 0.03, 0.05) thin films increase along with the niobium contents before 0.03 and decrease afterwards, which can be explained by the following two possible reasons. Firstly, the residual stress, either tensile or compressive, in the ferroelectric thin film significantly affects their physical and electrical properties [28]. The P_r
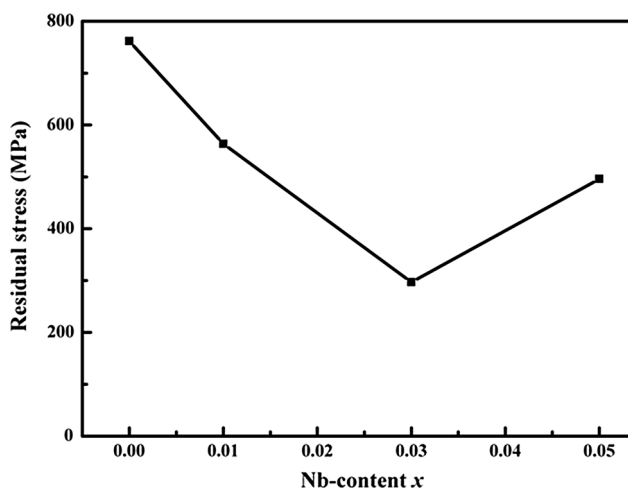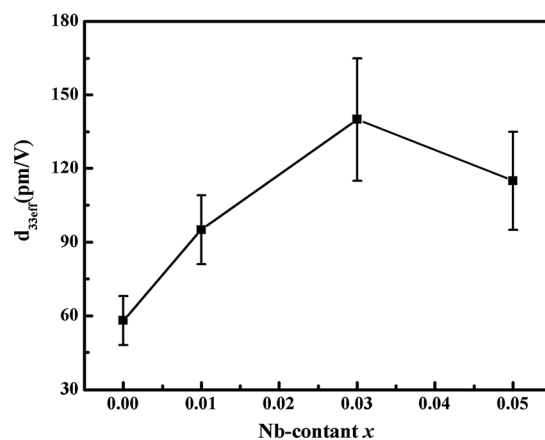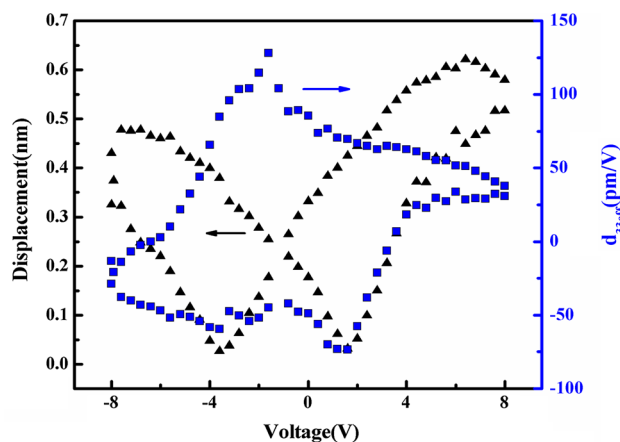
Fig. 5 The residual stresses values of the NKBT-N100x ($x = 0$, 0.01, 0.03, 0.05) thin films dependence of the niobium content

Fig. 6 P–E curves of the NKBT-N100x ($x = 0$, 0.01, 0.03, 0.05) thin films

Fig. 7 Local piezoelectric response as a function of applied voltage **a** "butterfly" D–V loop and **b** effective piezoelectric d_{33eff}–V hysteresis loop of the NKBT-5N thin film

was also reported to increase with increasing compressive stress and to decrease with increasing tensile stress [31]. Therefore the change tendency of residual stress for the NKBT-N100x ($x = 0$, 0.01, 0.03, 0.05) thin films led to the change of their P_r values. Secondly, the P_r value of the NKBT-5N thin film decreases because of the significant impairment effect of the non-ferroelectric $Bi_2Ti_2O_7$ phase.

The typical "butterfly" displacement–voltage (D–V) loop and effective piezoelectric coefficient-voltage (d_{33eff}-V) hysteresis loop of the NKBT-5N thin film as a function of applied voltage are plotted in Fig. 7. The PFM tip was fixed above the thin films by a dc voltage from -8 to 8 V to measure the piezoresponse signal. The maximum d_{33eff} value of the NKBT-5N thin film are estimated to be 128 pm/V, and the statistically averaged d_{33eff} value are 115 pm/V for 10 piezoelectric measurements. This value is larger than that of NBT-BT thin film (94 pm/V) and is

comparable to the piezoelectric response of 80–100 pm/V of PZT thin films [22]. Similarly, the statistic d_{33eff} values of NKBT-N100x ($x = 0$, 0.01, 0.03) thin films are 58, 95 and 140 pm/V respectively. The variation tendency of the statistic d_{33eff} values of NKBT-N100x ($x = 0$, 0.01, 0.03, 0.05) thin films is also caused by the residual stresses. In thin films, out-of-plane displacements induced by a driving field in the three directions must be accompanied by a contraction in the 1–2 planes. Superimposing a high biaxial tensile stress in the 1–2 plane severely limits the amount of allowed contraction and thus reduces the potential out-of-plane strains possibly through electrical loading [32]. Therefore, lower d_{33eff} values will be measured for thin films with high residual tensile stresses.

Figure 8 shows the leakage current density of the NKBT-N100x ($x = 0$, 0.01, 0.03, 0.05) thin films measured at room temperature. The NKBT-N100x thin films show a decreased leakage current density compared with the NBT-BT thin films [33]. The higher-valence ion of Nb^{5+} substituting for Ti^{4+} at B site had the advantage of decreasing the number of oxygen vacancies. When Nb^{5+}
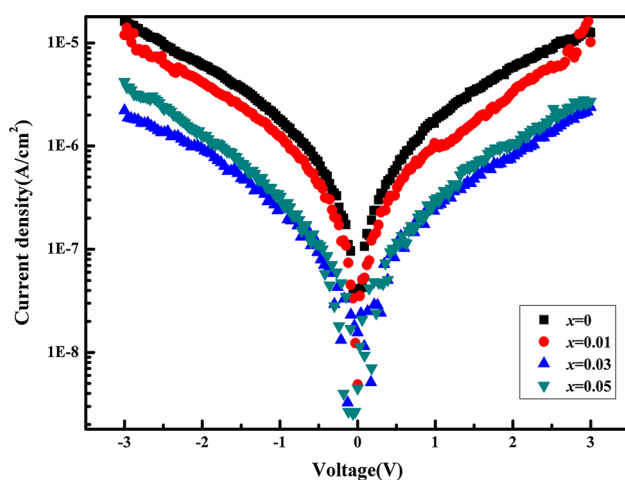
Fig. 8 *I–V* curves of the NKBT-N100*x* (*x* = 0, 0.01, 0.03, 0.05) thin films

replaces Ti^{4+}, the acceptor and donor can be represented by the following defect reactions [34]:

$$Ti \xrightarrow{Nb^{5+}} Nb_{Ti}^{\cdot} + e^{'} \qquad (5)$$

$$O_2 + 2V_O^{''} + 4e^{'} \longrightarrow 2O_O \qquad (6)$$

For Nb^{5+} substituting for Ti^{4+}, one positive charge center in Ti sites and one electron will be created under charge neutrality restrictions. The electron neutralizes the influence of the intrinsic oxygen vacancies, which leads to lower conductivity. Therefore, the improvement of electrical properties due to the Nb-doping was attributed to the decreased number of intrinsic oxygen vacancies. However, the leakage current density of the NKBT-5N thin film was increased because of the too much Nb-doping contents. As it was further increased, the higher valent substituents should cause an excess of electrons over intrinsic oxygen vacancies, which leads to the increase of the leakage current density of the NKBT-5N thin film.

4 Conclusions

The effects of niobium content on the microstructures, mechanical and electric properties of NKBT-N100*x* (*x* = 0, 0.01, 0.03, 0.05) thin films deposited on Pt/Ti/SiO$_2$/Si (100) have been investigated in detail. The NKBT-3N thin film has the largest ferroelectric and piezoelectric property, the smallest leakage current, elasticity modulus (102 Gpa), hardness (5.1 Gpa) and residual stress (297 Mpa) among the NKBT-N100*x* (*x* = 0, 0.01, 0.03 and 0.05) thin films.

References

1. L.E. Cross, Nature **432**, 24–25 (2004)
2. G.A. Smolenskii, A.I. Agranovskaya, N.N. Krainik, Sov. Phys. Solid State **2**, 2651–2654 (1961)
3. T. Takenaka, K. Sakata, Jpn. J. Appl. Phys. **30**, 2236–2239 (1991)
4. K. Sakata, Y. Masuda, Ferroelectrics **7**, 347–349 (1974)
5. T. Takenaka, T. Okuda, K. Takegahara, Ferroelectrics **196**, 175–178 (1997)
6. I. Hideki, H.N.T. Tadashi, Jpn. J. Appl. Phys. **40**, 5660–5663 (2001)
7. M. Cerne, A. Catalin, G.P. Ioncea, J. Mater. Sci. **46**, 5621–5627 (2011)
8. P. Fu, Z.J. Xu, R.J. Chu, Mater. Sci Mater. Electron. **23**, 2167–2172 (2012)
9. Y. Zhang, J. Li, B. Zhang, J. Am. Ceram. Soc. **91**, 2716–2719 (2008)
10. J.E. Daniels, W. Jo, J. Rodel, Acta Mater. **58**, 2103–2111 (2010)
11. Y.Q. Gong, J. Phys. D Appl. Phys. **45**, 305301 (2012)
12. K. Kumar, B.K. Singh, N. Sinha, Ceram. Inter. **37**, 2997–3004 (2011)
13. D.M. Lin, D.Q. Xiao, J. Zhu, Appl. Phys. Lett. **88**, 062901–062903 (2006)
14. Q. Xu, M. Chen, W. Chen, Acta Mater. **56**, 642–650 (2008)
15. S.T. Zhang, B. Yang, W.W. Cao, Acta Mater. **60**, 469–475 (2012)
16. K. Kumar, B. Kumar, Ceram. Inter. **38**, 1157–1165 (2012)
17. W.C. Oliver, G.M. Pharr, J. Mater. Res. **7**, 1564–1583 (1992)
18. B.D. Cullity, *Elements of X-Ray Diffraction* (Addison-Wesley, Reading, MA, 1978)
19. B.J. Fu, Y.C. Zhang, M.J. Hong, Mater. Sci Mater. Electron. **24**, 3240–3243 (2013)
20. E. Preeyakarn, J. Sukanda, W.J. Anucha, Microsc. Soc. Thail. **5**(1–2), 55–57 (2012)
21. S.K. Singh, H. Ishiwara, Thin Solid Films **497**, 90–95 (2006)
22. D.Z. Zhang, X.J. Zheng, Y.Q.J. Gong, Alloys Compd. **504**, 129–133 (2010)
23. R.C. Buchanana, T.R. Armstrong, R.D. Roseman, Ferroelectrics **135**, 343–369 (1992)
24. K. Pengpat, P. Jarupoom, T. Tunkasiri, Curr. Appl. Phys. **8**, 241–245 (2008)
25. X.J. Zheng, J.Y. Li, Y.C. Zhou, Acta Mater. **52**, 3313–3322 (2004)
26. C. Wang, H. Elastic, Mater. Lett. **58**, 1557–1560 (2004)
27. S. Yoshiki, T. Toshihiko, Ferroelectrics **224**, 365–372 (1999)
28. J.F. Li, Z.X. Zhu, F.P. Lai, J. Phys. Chem. C **114**, 17796–17801 (2010)
29. K. Omoto, S.T. Norberg, S. Hull, J. Solid State Chem. **183**, 392–401 (2010)
30. T. Yu, K. Kwok, H.L.W. Chan, Mater. Lett. **61**, 2117–2120 (2007)
31. T. Kumazawa, Y. Kumagai, H. Miura, Appl. Phys. Lett. **72**, 608–610 (1998)
32. T.A. Berfield, R.J. Ong, D.A. Payne, J. Appl. Phys. **101**, 024102–024107 (2007)
33. Y. Guo, M. Ishida, M. Gu, Solid State Commun. **149**, 14–17 (2009)
34. Z. Zhou, X. Dong, H. Yan, J. Appl. Phys. **100**, 044112–044115 (2006)